Meteoritics & Planetary Science 41, Nr 1, 67–81 (2006)
Abstract available online at http://meteoritics.org

Petrographic comparison of refractory inclusions from different chemical groups of chondrites

Y. LIN[1, 3*], M. KIMURA[2], B. MIAO[1], D. DAI[3], and A. MONOI[2]

[1]State Key Laboratory of Lithospheric Evolution, Institute of Geology and Geophysics, Chinese Academy of Sciences, Beijing, China
[2]Faculty of Science, Ibaraki University, Mito 310-8512, Japan
[3]Guangzhou Institute of Geochemistry, Chinese Academy of Sciences, Guangzhou, China
*Corresponding author. E-mail: linyt@mail.igcas.ac.cn

(Received 31 January 2005; revision accepted 05 July 2005)

Abstract–Twenty-four refractory inclusions (40–230 μm, with average of 86 ± 40 μm) were found by X-ray mapping of 18 ordinary chondrites. All inclusions are heavily altered, consisting of fine-grained feldspathoids, spinel, and Ca-pyroxene with minor ilmenite. The presence of feldspathoids and lack of melilite are due to alteration that took place under oxidizing conditions as indicated by FeO-ZnO-rich spinel and ilmenite. The pre-altered mineral assemblages are dominated by two types: one rich in melilite, referred to as type A-like, and the other rich in spinel, referred to as spinel-pyroxene inclusions. This study and previous data show similar type and size distributions of refractory inclusions in ordinary and enstatite chondrites.

A survey of refractory inclusions was also conducted on Allende and Murchison in order to make unbiased comparison with their counterparts in other chondrites. The predominant inclusions are type A and spinel-pyroxene, with average sizes of 170 ± 130 μm (except for two mm-sized inclusions) in Allende and 150 ± 100 μm in Murchison. The relatively larger sizes are partially due to common conglomerating of smaller nodules in both chondrites. The survey reveals closely similar type and size distributions of refractory inclusions in various chondrites, consistent with our previous data of other carbonaceous chondrites. The petrographic observations suggest that refractory inclusions in various groups of chondrites had primarily formed under similar processes and conditions, and were transported to different chondrite-accreting regions. Heterogeneous abundance and distinct alteration assemblages of refractory inclusions from various chondrites could be contributed to transporting processes and secondary reactions under different conditions.

INTRODUCTION

Refractory inclusions (RIs) are the most extensively studied components of carbonaceous chondrites, and they are classified into various petrographic types. Most of coarse-grained RIs are compact type A (melilite-spinel-rich), type B (melilite-fassaite-rich), type C (anorthite-fassaite-rich) and POI (plagioclase-olivine-rich), and they were usually reported in CV3 chondrites (e.g., Grossman 1975; Wark and Lovering 1982; Wark 1987; Sheng et al. 1991). In contrast, hibonite-rich inclusions are the intensely studied objects in CM2 chondrites (e.g., Macdougall 1979; MacPherson et al. 1983; Ireland 1990; Simon et al. 1998), whereas grossite-bearing inclusions appear more abundant in CR clan chondrites (e.g., Kimura et al. 1993; Weber and Bischoff 1997; Aléon et al. 2002; Krot et al. 2002). Fine-grained anorthite-spinel-rich inclusions (ASI) were reported in the Ningqiang carbonaceous chondrite (Lin and Kimura 1998), with their counterparts in CR chondrites (Weber and Bischoff 1997; Aléon et al. 2002), reduced CV chondrites (Krot et al. 2004a), Yamato-81020 (CO3) (Itoh et al. 2004) and the unique Acfer 094 carbonaceous chondrite (Krot et al. 2004b). In addition, fine-grained spinel-pyroxene and melilite-spinel-rich (fluffy type A) inclusions have been widely reported from CV chondrites. It seems that various groups of carbonaceous chondrites are characteristic of distinct petrographic types and sizes of RIs. However, it is noticed that most of these RIs were artificially selected, especially those from CV and CM chondrites, and they are unrepresentative.

On the other hand, RIs are usually rare in ordinary and enstatite chondrites. Furthermore, they are typically small in size and heavily altered (Bischoff and Keil 1984; Fagan et al. 2000; Guan et al. 2000c; Kimura et al. 2002; Lin et al. 2003).

However, RIs in both ordinary and enstatite chondrites commonly share similar ^{16}O-rich oxygen isotopic compositions (McKeegan et al. 1998; Guan et al. 2000a; Fagan et al. 2001; Kimura et al. 2002; Lin et al. 2003), the canonical initial (^{26}Al/^{27}Al) ratio of ~5 × 10^{-5} (Guan et al. 2000c; Huss et al. 2001; Lin et al. 2003) and rare earth element patterns (Guan et al. 2002; Lin et al. 2003) as the counterparts in carbonaceous chondrites, suggesting their similar origins as those from carbonaceous chondrites.

In order to investigate distribution of RIs in different groups of chondrites, unbiased surveys of RIs are required. However, such a survey was carried out only on few chondrites, including ordinary and enstatite chondrites (Bischoff and Keil 1984; Fagan et al. 2000; Guan et al. 2000c; Kimura et al. 2002; Lin et al. 2003), and some CR clan chondrites (Weber and Bischoff 1997; Krot et al. 2001; Krot et al. 2006) and some unique carbonaceous chondrites (Russell et al. 2000; Krot et al. 2004b). As a part of our systematic study of RIs from various groups of chondrites, we report here petrography and mineral chemistry of 25 RIs from 18 unequilibrated ordinary chondrites. In addition, a survey of RIs was also conducted on Allende and Murchison, the most intensely studied CV3 and CM2 chondrites, respectively. With all available data of RIs in other enstatite, ordinary and carbonaceous chondrites, we compare petrographic types and sizes of RIs in various chemical groups of chondrites in order to clarify their genetic linkage. Although amoeboid olivine aggregates (AOAs), especially those containing spinel ± anorthite ± Ca pyroxene, probably formed in the same processes of refractory inclusions but at lower temperatures (e.g., Lin and Kimura 2003; Krot et al. 2004c), these assemblages are not included in this study because a survey for AOAs in ordinary and enstatite chondrites is rather difficult to perform. The preliminary results were reported by Lin et al. (2004).

SAMPLES AND EXPERIMENTAL PROCEDURES

One polished thin section was made from each of 8 chondrites collected in Grove Mountains, Antarctica, including 6 L3s (GRV 99001, 99019, 99020, 99021, 99022, and 99026) and 2 H4s (GRV 99011, 99028), 4 sections from Allende (CV3) and 2 sections from Murchison (CM2). Another 10 polished thin sections from the National Institute of Polar Research, Japan, are 5 H3s (Asuka-882004, Yamato-75028, 790461, 791428, 791500), 4 L3s (ALH 77216, Yamato-791961, 793375, and 82055) and 1 LL3 (Yamato-791558). In addition, a section of Yamato-81020 (CO3) is also observed in this study. Surface areas of these sections are summarized in Table 1.

Surveys for RIs were conducted on all sections of the unequilibrated ordinary chondrites (UOCs), using an electronic probe microanalyzer (EPMA) of JEOL 733 type in the Ibaraki University, Mito, Japan, with a defocused beam (50 μm in diameter) and following the method described by Lin et al. (2003). The candidates of RIs were confirmed using the same EPMA. High-resolution photomosaic of backscattered electron (BSE) images of the sections of Allende and Murchison were made using another EPMA of type JEOL 8100 in the Guangzhou Institute of Geochemistry, Chinese Academy of Sciences, and RIs were found on the photomosaics and confirmed using the same instrument. Quantitative analyses of minerals and bulk compositions were carried out using the EPMA in the Ibaraki University or that in the Guangzhou Institute of Geochemistry. The operating conditions for the analyses of minerals were 15 kV accelerating voltage, 20 nA beam current and 30 s counting time with a focused beam, and those for the bulk compositions were the same except for a defocused beam with a diameter of 20–50 μm depending on sizes of the RIs. Natural and synthetic minerals were used as standards. Overlaps of the K_α lines of V and Mn by the K_β lines of Ti and Cr, respectively, were corrected using a deconvolution program after Lin et al. (2003). Both focused and defocused beam analyses were corrected by the Bence-Albee method.

RESULTS

Refractory Inclusions in Ordinary Chondrites

Petrography

A total of 18 RIs were found in 6 H chondrites (2 in Yamato-75028, 2 in Yamato-791500, 3 in Yamato-790461, 4 in GRV 99011, and 7 in Yamato-791428), but none in the other 12 H chondrites, indicating high heterogeneity of RIs among ordinary chondrites. Sizes of these RIs range from 53 to 138 μm in diameter with an average of 86 ± 26 μm. All of them contain secondary fine-grained feldspathoids possibly replacing melilite. If so, the original mineral assemblages of these RIs consist mainly of melilite and spinel, similar to melilite-spinel-rich (type A) or spinel-pyroxene inclusions in carbonaceous chondrites. Accordingly, those with small grains of spinel embedded in the fine-grained alteration assemblages are referred to as type A-like (12), and others with relatively larger and irregular lumps of spinel surrounded by thin layers of the alteration assemblages to as spinel-pyroxene (5) inclusions. Another inclusion is referred to as fassaite-rich fragment. The type A-like inclusions consist mainly of fine-grained alteration assemblages, spinel and Ca-pyroxene. The spinel occurs as small and irregular to subhedral grains dispersed in the alteration assemblages (Fig. 1a). Ca pyroxene occurs as relicts of Wark-Lovering rims. Other minor minerals are ilmenite as small grains in spinel in 2 RIs and hibonite as laths in the alteration assemblage in 1 RI. The ilmenite most likely replaces perovskite. In contrast, the spinel-pyroxene inclusions consist predominantly of spinel that occurs as large and anhedral grains (Fig. 1b). Thin rims of fine-grained alteration

Table 1. Summary of refractory inclusions in various chondrites.

Groups	EH3	Ordinary chondrite		CO3			CM2		CV3		CV3-like	CR	CH	Unique	CO/CM
Meteorites	Sahara 97159	Yamato-792947	Others	GRV 021579	Yamato-81020	Others	Murchison	GRV 020025	Allende	GRV 022459	Ningqiang		NWA 739	Acfer 094	MAC 87300, 88107
Section number	2	5	18	1	1	10	2	1	4	1	21	12	1	1	2
Total areas (mm^2)	310	267	1390	62	6.1	858	210	120	1090	29	1740		100	34	270
Type A/A-like	35	15	14	4	42	51	9	6	40	3	31	14	14	95	55
Sp-Px/Sp fragment[a]	26	20	9	8	23	145	7	5	20		79		13		174
ASI/AnPx[a]					22	1					7	5		14	
Gro/Hib-rich[a]						6			1			4	23	19	2
Sp/Hib/Fas[a]															
Spherule/ fragment	5	2	1	1	1	12	1	1	1					1	
B/C/POI[a]	2										6			3	
Total	68	37	24	13	88	215	17	12	62	3	123	23	50	132	231
Reference[b]	2	3	1	1	1	4	1	5	1	5	6	7	8	9	10

[a]Abbreviations: Sp: spinel, Px: Ca-pyroxene, An: anorthite, Hib: hibonite, Fas: fassaite, B: type B, C: type C, ASI: anorthite-spinel-rich, POI: plagioclase-olivine-rich.

[b]1 = this work, 2 = Lin et al. (2003), 3 = Kimura et al. (2002), 4 = Russell et al. (1998), 5 = Dai et al. (2004), 6 = Lin and Kimura (2003), 7 = Aléon et al. (2002), 8 = Krot et al. (2006), 9 = Krot et al. (2004b), 10 = Russell et al. (2000).

Table 2. Bulk compositions of refractory inclusions in ordinary chondrites (normalized to 100 wt%).

RI	Type	Section	Group	SiO_2	TiO_2	Al_2O_3	Cr_2O_3	FeO	MnO	MgO	CaO	Na_2O	K_2O	P_2O_5	SO_3	Cl
CAI-14	A-like	Y-75028	H3	17.9	2.00	41.0	0.09	17.7	0.06	9.21	2.49	4.90	1.59	0.00	3.03	0.00
CAI-15	A-like	Y-75028	H3	27.4	0.63	31.6	0.00	12.9	0.00	3.89	1.13	11.9	2.88	0.00	6.50	1.20
CAI-02	A-like	Y-790461	H3.4	14.2	2.52	47.5	0.58	16.5	0.12	11.1	0.96	4.93	0.48	0.00	0.14	1.07
CAI-03	A-like	Y-790461	H3.4	23.8	0.77	36.7	4.69	10.3	0.10	9.19	2.03	9.74	0.62	0.00	0.10	1.93
CAI-04	A-like	Y-791428	H3	16.8	0.24	39.4	13.2	15.1	0.17	8.20	4.26	2.18	0.22	0.00	0.14	0.07
CAI-05	A-like	Y-791428	H3	23.1	2.24	32.8	8.32	17.5	0.09	4.30	1.77	8.03	1.40	0.00	0.21	0.18
CAI-06	A-like	Y-791428	H3	39.0	0.47	22.6	6.78	12.5	0.07	3.59	4.03	9.02	1.20	0.00	0.24	0.48
CAI-07	A-like	Y-791428	H3	11.0	0.99	27.6	23.6	17.0	0.29	6.19	2.63	7.19	0.33	2.33	0.00	0.96
CAI-08	A-like	Y-791428	H3	10.0	0.28	29.2	12.5	36.3	0.21	9.02	0.45	1.36	0.19	0.00	0.35	0.23
CAI-10	A-like	Y-791428	H3	13.4	2.49	22.2	24.7	23.1	0.37	4.44	0.47	7.19	0.40	0.00	0.29	1.00
CAI-11	A-like	Y-791428	H3	14.3	0.55	31.5	14.0	23.7	0.21	10.5	2.99	1.45	0.27	0.00	0.41	0.13
CAI-13	A-like	A-77216	L3	27.4	0.30	24.8	12.4	13.0	0.15	5.67	7.75	3.41	0.12	4.64	0.33	0.03
CAI-16[a]	A-like	Y-793375	L3	44.2	0.98	23.3	2.47	4.56	0.00	6.48	7.70	8.27	1.22	0.00	0.00	0.79
CAI-18	Sp-frag	Y-791500	H3.4	17.0	5.29	40.5	4.75	13.9	0.20	12.9	2.25	2.51	0.16	0.00	0.37	0.07
CAI-20	Sp-frag	Y-791500	H3.4	16.8	0.49	27.4	22.7	20.7	0.31	6.78	1.71	2.73	0.02	0.00	0.24	0.03
CAI-01	Fas-frag	Y-790461	H3.4	37.1	2.40	24.9	0.56	2.48	0.00	9.57	22.9	0.08	0.00	0.00	0.00	0.00

[a]Average of two analyses.

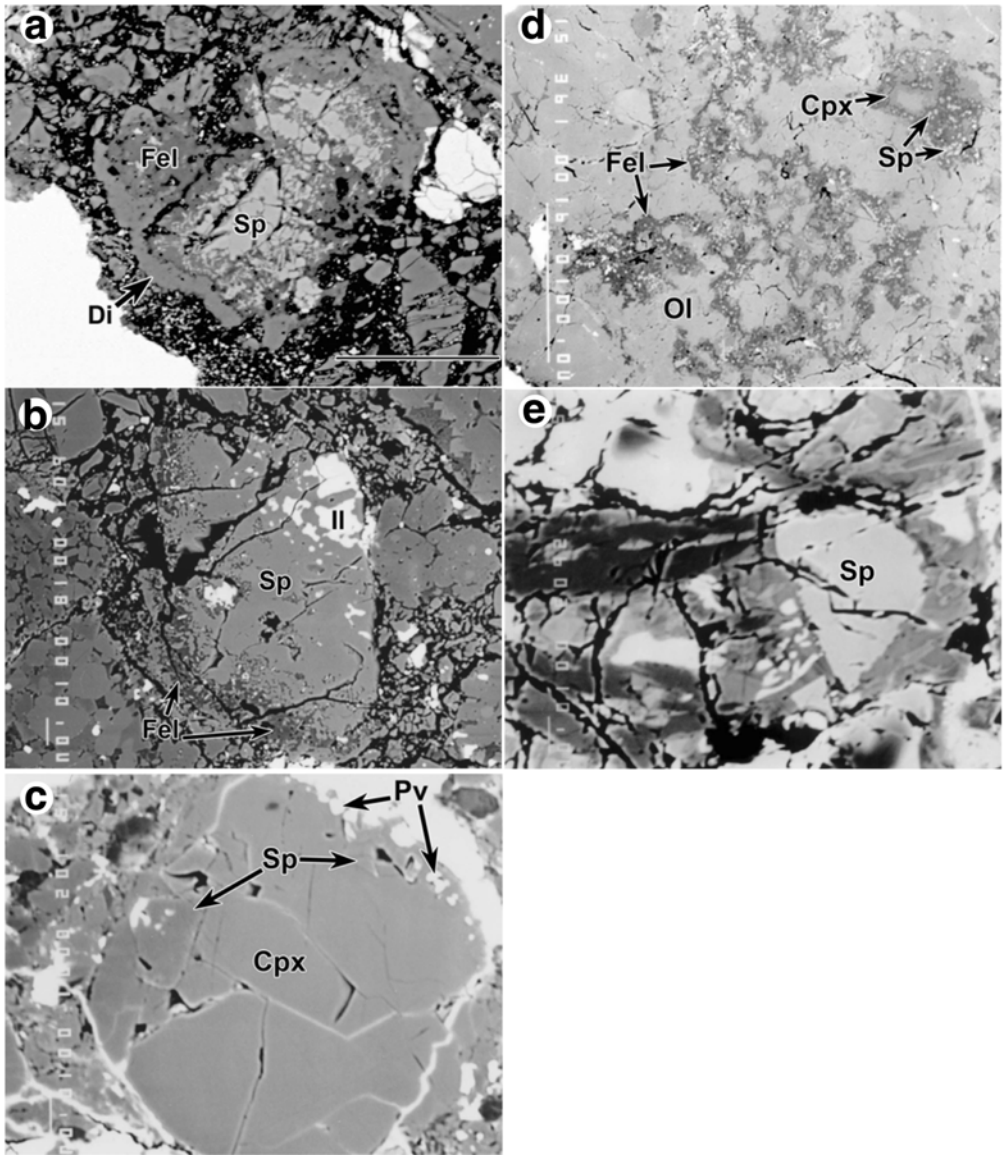

Fig. 1. Backscattered electron images of RIs in ordinary chondrites. a) Type A-like inclusion in GRV 99011 (H4), consisting of a core of spinel (Sp) and fine-grained alteration assemblages (Fel) and a thin diopside (Di) rim. Width of 120 μm. b) Spinel-rich fragment in Yamato-791500 (H3.4), enclosing ilmenite (Il) mainly at one side. Fine-grained alteration assemblages (Fel) at the other side. Width of 170 μm. c) Fassaite-rich fragment in Yamato-790461 (H3.4), consisting of several subhedral grains of fassaite (Cpx) with fine-grained ilmenite (Il) and spinel at the rims. Width of 120 μm. d) Type A-like in Yamato-793375 (L3), convolute assemblage consisting of fine-grained spinel (bright spots) in alteration products (Fel) and thin Ca-pyroxene rims (Cpx). Width of 310 μm. e) Spinel-rich fragment in GRV 99026 (L3). Width of 130 μm.

assemblages are partly around the spinel grains. Small grains of ilmenite are enclosed in spinel, similar to the occurrence of perovskite in spinel in spinel-pyroxene inclusions. Figure 1c shows the unique fassaite-rich fragment, consisting of several subhedral to anhedral grains of fassaite with a few small inclusions of ilmenite and spinel along the boundaries.

Only 6 RIs were found in 4 L3 chondrites (1 in each of ALHA77216, Y-793375 and GRV 99001, and 3 in GRV 99026), and none in the other 6 L3s and the single LL3. Sizes of the RIs range from 40 to 70 μm in diameter, except for the largest one with a diameter of 230 μm. All of the RIs are strongly altered, as those in the H chondrites. Two of the RIs consist of fine-grained alteration assemblages and small grains of spinel (Fig. 1d), and they are referred to as type A-like. The other 4 inclusions are referred to as spinel-pyroxene inclusions, consisting mainly of spinel lumps (Fig. 1e). The petrographical types of these RIs are summarized Table 1.

Bulk Compositions

Thirteen of the RIs have been quantitatively analyzed for bulk compositions, and the results are listed in Table 2. Inclusion RI-16 was analyzed twice, and the deviations are

<6% for major elements and <13% for minors. It is noticed that all analyses show high contents of FeO (4.56–36.3 wt%), Na_2O (up to 11.9 wt%) and Cr_2O_3 (up to 24.7 wt%), but low in CaO content (0.4–7.8 wt%). Higher Cl contents (up to 0.8–1.9 wt%) were analyzed in Na_2O-rich RIs (>6.9 wt%), suggesting presence of sodalite. The bulk atomic ratios of Al, Si, Mg + Fe plot in the ranges of type A and spinel-pyroxene inclusions from the Ningqiang and Yamato-81020 carbonaceous chondrite (Fig. 2a). In contrast, these RIs are characteristic of Ca-poor and alkali-rich, similar to those in the Y-792947 (H3) with some plotted in the range of Sahara 97159 EH3 chondrite (Fig. 2b).

Mineral Chemistry

Spinel is the most common phase in these RIs and is large enough for quantitative analyses. All analyses are FeO-rich (>12.6 wt%). The contents of Cr_2O_3 range from below the detection limit (<0.03 wt%) up to 58.1 wt%, showing a continuous variation from Al_2O_3-rich spinel to Cr_2O_3-rich chromite. The Al/Al + Cr ratio is positively correlated with the Mg/Mg + Fe ratio (Fig. 3a). Most grains of the spinel are ZnO-bearing (up to 2.9 wt%), but there is no significant correlation between ZnO and FeO (Fig. 3b). In contrast, most FeO-rich grains (>23 wt%, hence chromite, instead of spinel) contain low ZnO (<1.2 wt%, except for two analyses of 1.55, 2.03 wt%). Other minor elements are V_2O_3 (<0.4 wt%) and MnO (0.1–0.9 wt%), and the latter appears to be correlated with the FeO content. Representative analyses are given in Table 3. Ca pyroxene contains high content of Al_2O_3 up to 19.9 wt%, but with low TiO_2 that is correlated with the former (Fig. 4). Fassaite in the fassaite-rich fragment is Al_2O_3-rich (22.8–23.6 wt%). The TiO_2 content decreases from 3.84 wt% at the rim with ilmenite and spinel to 1.27 wt% at the other side. Other minor elements are Cr_2O_3 (0.25–0.35 wt%) and FeO (<0.32 wt%) (Table 3). Ilmenite is small and only a few analyses are available. Besides TiO_2 (54.6–55.5 wt%) and FeO (38.8–39.4 wt%), it contains 4.75–4.91 wt% MgO and 1.22–1.32 wt% MnO (Table 3). Two analyses of hibonite in inclusion RI-5 show low TiO_2 (1.77–2.77 wt%) and MgO (1.62–2.07 wt%). Other components are Al_2O_3 (81.8–82.3 wt%), CaO (7.31–7.97 wt%), FeO (1.14–2.39 wt%) and Cr_2O_3 (0.43–1.79 wt%). Feldspathoids are too small to analyze quantitatively. Besides nepheline, there is sodalite indicated by presence of Cl.

Petrographic Type and Size Distributions

Because of the small number of RIs from ordinary chondrites, all 24 RIs are summarized together, with the petrographic type abundances listed in Table 1 and the size distribution plotted in Fig. 5. The average size of these RIs is 86 ± 40 μm. For comparison, petrographic type and size distributions of RIs from the three paired H3 chondrites (Yamato-792947, 793408, and 82038) are listed in Table 1 and plotted in Fig. 5, respectively, which are similar to those observed in this work, although these paired H3 chondrites contain unusually abundant RIs than other ordinary chondrites (Kimura et al. 2002).

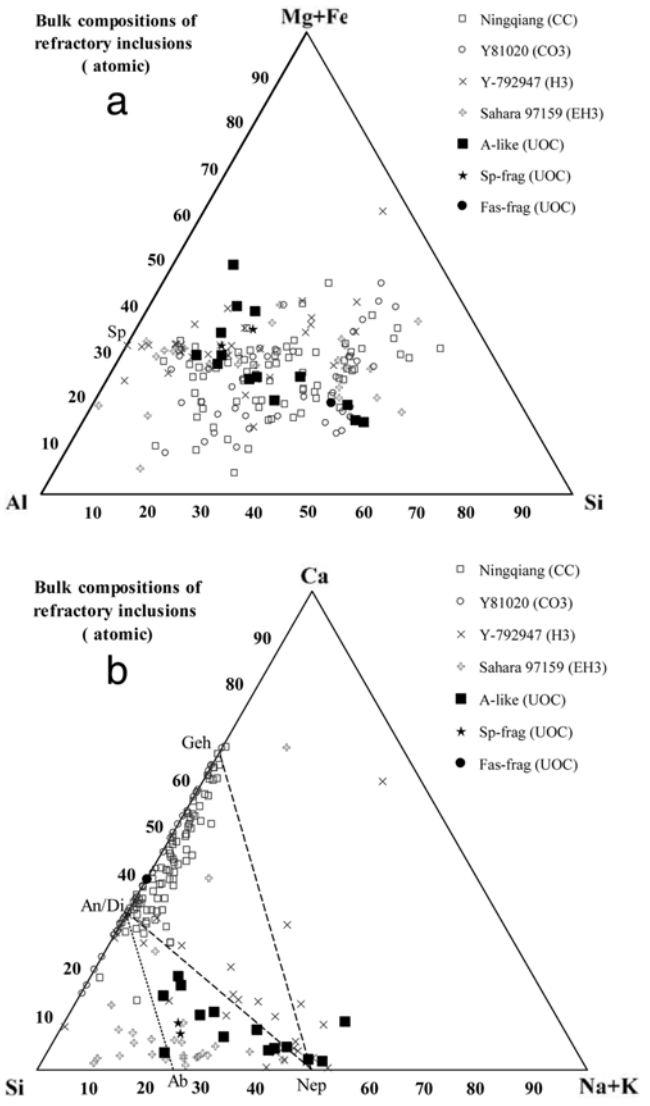

Fig. 2. Bulk compositions of RIs. a) Atomic ratios of Al, Si, Mg + Fe of the refractory inclusions in ordinary chondrites (filled symbols), mainly plotted close to joint line between spinel (Sp) and the endmember of Si with a few of the type A-like inclusions having higher Mg + Si values. b) Atomic ratios of Si, Na + K, Ca of the refractory inclusions in ordinary chondrites, showing higher contents of alkali and lower content of Ca in comparison with those in carbonaceous chondrites. Refractory inclusions in other chondrites are plotted for comparison. Abbreviation: Sp-frag: spinel-fragment, Fas-frag: fassaite-fragment, A-like: type A-like. Literature: Ningqiang (Lin and Kimura 2003), Y-792947 (Kimura et al. 2002), Sahara 97159 (Lin et al. 2003).

Refractory Inclusions in Murchison (CM2)

A total of 17 RIs were found in the two sections of Murchison. All of the RIs are heavily altered, with no melilite

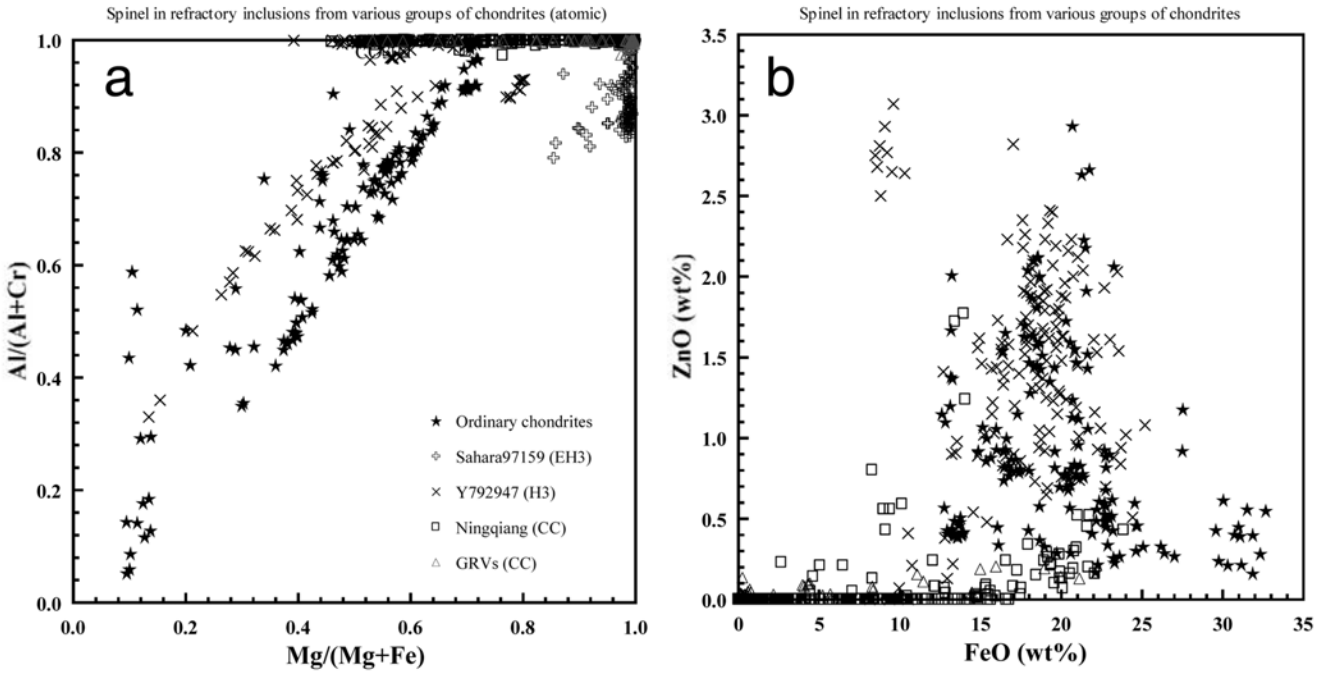

Fig. 3. Compositions of spinel. (a) Atomic ratios of Al/(Al + Cr) versus Mg/(Mg + Fe), showing a continuous variation from Mg-, Al-rich spinel to Fe-, Cr-rich chromite. This is similar to the previous result of Y-792947 (H3). Spinels in carbonaceous and enstatite chondrites show distinct trends. (b) FeO versus ZnO plots, showing high contents of FeO and ZnO of spinel in ordinary chondrites. However, there is no correlation between FeO and ZnO. It is noticed that the most FeO-rich grains contain lower ZnO. Literature: Ningqiang (Lin and Kimura 2003), Y-792947 (Kimura et al. 2002), Sahara 97159 (Lin et al. 2003), and GRV carbonaceous chondrites (Dai et al. 2004).

remaining. They consist mainly of fine-grained alteration assemblages, spinel and Ca pyroxene with minor perovskite and hibonite. Spinel is FeO-poor and the alteration assemblages are mainly phyllosilicates. If the alteration assemblages were formed from melilite, the pre-altered mineral assemblages of most RIs are similar to type A or spinel-pyroxene inclusions. Accordingly, 9 RIs are referred to as type A-like inclusions, with small grains of spinel in the alteration assemblages (Fig. 6a). Laths of hibonite were found only in one of the type A-like inclusions, coexisting with small grains of spinel both in alteration assemblages. Other 7 assemblages are referred to as spinel-pyroxene inclusions, having spinel cores and Ca-pyroxene rims (Fig. 6b). Most of the spinel-pyroxene inclusions have outer layers of olivine. Only one inclusion consists of Ca pyroxene with several euhedral grains of spinel, and it is referred to as spinel-fassaite fragment (Fig. 6c).

Sizes of the Murchison RIs range from 50 to 455 μm in diameter. However, as shown in Fig. 6, the largest spinel-pyroxene inclusion and others are assemblages of several individual concentric nodules. The size distribution of single inclusions and these nodules is plotted in Fig. 5d, with average of 151 ± 98 μm in diameter.

Refractory Inclusions in Yamato-81020 (CO3)

The size distribution of 88 RIs from Yamato-81020 is plotted in Fig. 5c, ranging from 25 to 275 μm with an average of 129 ± 72 μm. All of the RIs are free from alteration and contain no secondary minerals such as nepheline, sodalite, hedenbergite or ilmenite, as noticed in previous studies (Kojima et al. 1995; Itoh et al. 2004). This is consistent with the low bulk concentrations of Na_2O and K_2O of these RIs (Fig. 2b). Type A inclusions are the most abundant (39 out of 88). Besides melilite and spinel, other common phases are Ca pyroxene, perovskite, and anorthite. Grossite and hibonite were found only in 3 of them. Spinel-pyroxene inclusions are the second abundant (23 out of 88). All of them show concentric textures consisting of spinel cores and pyroxene rims with minor melilite and anorthite. Olivine was found in more than half of the spinel-pyroxene inclusions, as the outmost layers. A unique feature of Yamato-81020 is abundant anorthite-pyroxene-rich inclusions (22 out of 88). These inclusions consist mainly of anorthite and Ca pyroxene, and 9 of them contain spinel (Fig. 6d). Except for the low content or lack of spinel, the anorthite-pyroxene-rich inclusions are similar to the anorthite-spinel-rich inclusions (ASIs) in the Ningqiang carbonaceous chondrite, and the latter were proposed to be produced by alteration of type As with melilite replaced by anorthite and Ca pyroxene (Lin and Kimura 1998). The other 3 refractory inclusions are grossite-rich (2) and fassaite-rich (1) assemblages.

Refractory Inclusions in Allende (CV3)

Sixty-two RIs were found in 4 sections of Allende. Most

Table 3. Selected analyses of spinel and Ca pyroxene in ordinary chondrites, in wt%.

	Spinel								Ca pyroxene							
	Type A-like					Sp. frag.[a]		Fas. frag.	Type A-like					Fas. frag.		
	1	2	3	4	5	7	8	6	9	10	11	12	13	14[b]	15	16
SiO_2	n.d.	n.d.	n.d.	n.d.	n.d.	n.d.	n.d.	0.07	51.9	55.1	51.4	52.6	54.4	39.1	39.5	41.0
TiO_2	0.20	n.d.	n.d.	0.25	0.11	0.26	0.08	0.09	0.75	n.d.	1.04	0.10	0.21	3.72	3.20	1.27
Al_2O_3	35.5	52.1	65.7	26.2	37.7	43.1	59.3	64.6	5.84	0.95	5.65	0.65	1.99	23.4	23.0	23.0
Cr_2O_3	31.7	14.9	0.03	42.0	30.6	25.3	8.68	1.44	0.12	0.09	0.60	0.46	0.13	0.28	0.28	0.25
V_2O_3	0.18	n.d.	0.23	0.21	0.18	0.24	0.26	0.12	n.d.	n.d.	n.d.	n.d.	n.d.	0.05	n.d.	n.d.
FeO	22.8	15.3	17.7	22.7	20.2	18.0	13.9	13.2	0.73	0.86	1.59	5.95	1.05	0.16	0.13	0.28
MnO	0.43	0.29	0.13	0.57	0.45	0.34	0.23	0.11	n.d.	n.d.	n.d.	0.18	n.d.	n.d.	n.d.	n.d.
MgO	8.62	15.1	15.3	8.32	10.7	13.2	17.6	17.8	16.5	18.0	15.3	15.8	17.1	8.84	8.85	9.36
CaO	0.04	n.d.	n.d.	n.d.	n.d.	n.d.	n.d.	0.22	25.1	25.2	23.7	21.9	25.2	25.4	25.5	25.7
ZnO	0.82	0.86	1.70	0.49	0.78	0.43	0.41	2.01	n.d.	n.d.	n.d.	n.d.	n.d.	n.d.	n.d.	n.d.
Na_2O	n.d.	n.d.	0.03	n.d.	n.d.	n.d.	n.d.	n.d.	0.04	0.14	1.12	0.40	0.09	n.d.	n.d.	n.d.
Total	100.2	98.5	100.8	100.7	100.7	100.8	100.5	99.7	100.9	100.3	100.4	98.1	100.1	100.9	100.4	100.9
	Cation per formula															
Si	0.000	0.000	0.000	0.000	0.000	0.000	0.000	0.002	1.862	1.983	1.851	1.972	1.968	1.417	1.438	1.478
Ti	0.005	0.000	0.000	0.006	0.002	0.005	0.002	0.002	0.020	0.000	0.028	0.003	0.006	0.102	0.087	0.035
Al	1.253	1.685	1.992	0.957	1.297	1.430	1.818	1.953	0.247	0.040	0.240	0.029	0.085	1.000	0.986	0.979
Cr	0.752	0.322	0.000	1.032	0.707	0.563	0.179	0.029	0.003	0.003	0.017	0.014	0.004	0.008	0.008	0.007
V	0.004	0.001	0.005	0.005	0.004	0.005	0.006	0.002	0.000	0.000	0.000	0.000	0.000	0.002	0.000	0.000
Fe	0.571	0.352	0.381	0.589	0.494	0.424	0.302	0.284	0.022	0.026	0.048	0.187	0.032	0.005	0.004	0.008
Mn	0.011	0.007	0.003	0.015	0.011	0.008	0.005	0.002	0.000	0.000	0.000	0.006	0.000	0.000	0.000	0.000
Mg	0.385	0.616	0.584	0.385	0.468	0.556	0.681	0.680	0.880	0.966	0.822	0.880	0.922	0.478	0.480	0.502
Ca	0.001	0.000	0.000	0.000	0.000	0.000	0.000	0.006	0.962	0.971	0.916	0.880	0.977	0.989	0.996	0.991
Zn	0.018	0.018	0.032	0.011	0.017	0.009	0.008	0.038	0.000	0.000	0.000	0.000	0.000	0.000	0.000	0.000
Na	0.000	0.000	0.001	0.000	0.000	0.000	0.000	0.001	0.003	0.010	0.079	0.029	0.006	0.000	0.000	0.000
Sum	3.000	3.000	3.000	3.000	3.000	3.000	3.000	3.000	4.000	4.000	4.000	4.000	4.000	4.000	4.000	4.000

[a] Abbreviations: Sp.= spinel, frag.= fragment.

[b] 14: at the rim enclosing spinel and ilmenite; 15: the core of fassaite fragment; 16: at the rim in contact with matrix of the meteorite.

n.d. = below detection limit (1σ, wt%): 0.02 for SiO_2, TiO_2, V_2O_3, CaO, and Na_2O; 0.04 for MnO; 0.08 for ZnO.

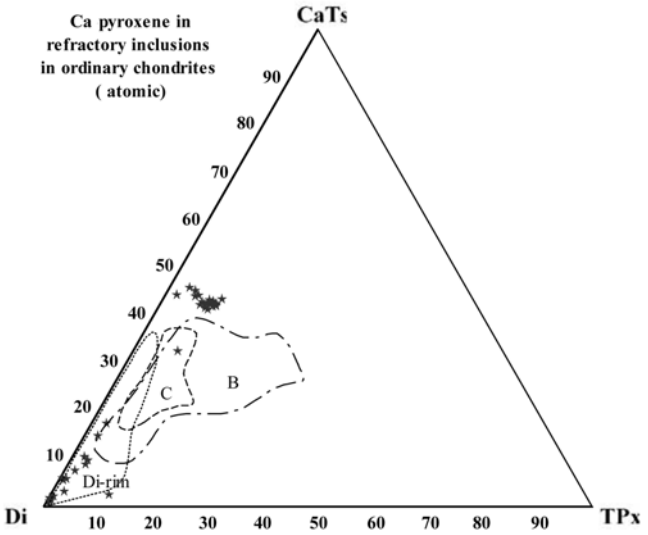

Fig. 4. Compositions of Ca pyroxene. A few available analyses are plotted in the range of Wark-Lovering rim (Di-rim). Other analyses with high contents of Ca-Tschermak ($CaAl_2SiO_6$) are an EPMA profile of the fassaite-fragment. Abbreviations: Di-diopside, TPx-Ti pyroxenes ($CaTi^{3+}AlSiO_6$ + $CaTi^{4+}Al_2O_6$). The ranges of Di rim and types B and C are from Lin and Kimura (2003).

of them (60 out of 62) are type A RIs and spinel-pyroxene. Five type A RIs show compact textures with euhedral and large grains (up to 20 μm) of spinel embedded in melilite, similar to compact type As (CTAs). Sizes of the CTAs are 205, 269, 370, 606, and 1090 μm in diameter, respectively. Melilite in the CTAs show little alteration. In contrast, other 35 type A RIs are heavily altered, with most melilite replaced by fine-grained alteration assemblages (mainly nepheline and sodalite). Other minor minerals are Ca pyroxene, perovskite, and/or ilmenite and hibonite. They are referred to as fluffy type As (MacPherson and Grossman 1984). Apparent diameters of FTAs range from 40 to 730 μm, except for the largest one with a diameter of 2.0 mm. Many of the larger inclusions are assemblages of several individual nodules. Spinel-pyroxene inclusions are the second abundant (20 out of 62). Some of them have outmost layers of olivine. One RI (58 μm) consists of laths of hibonite and spinel, with minor ilmenite and hedenbergite, probably a fragment of the spinel-hibonite spherule. Another inclusion (68 μm) mainly consists of hibonite, fassaite, and fine-grained feldspathoids with less abundant spinel, referred to as hibonite-rich inclusion. Similar to the RIs in other chondrites described above, size distribution of the single inclusions and the individual nodules of those conglomerated ones is plotted in Fig. 5g, except for the two largest mm-sized inclusions.

Refractory Inclusions in the Ningqiang Carbonaceous Chondrite

One hundred twenty-three RIs have been found in Ningqiang during our series studies of this carbonaceous chondrite (Lin and Kimura 2003). The size distribution of these RIs is plotted in Fig. 5f, showing a peak at about 200 μm in diameter. A few of RIs are millimeter-sized, and some of them are assemblages of numerous concentric nodules. Figure 6e shows size distribution of the nodules in one of such large assemblages, labeled as NQJ3-3#4. The average diameters of the nodules are 54 ± 48 μm, closely similar to those of RIs in ordinary and enstatite chondrites. Six coarse-grained RIs are probably once melted (3 type Bs, 2 POIs and 1 type C), and they are not included in the above size distribution.

DISCUSSION

Distinct Alteration Features

Alteration of the RIs is clearly related to chemical groups of the host chondrites. All RIs in the ordinary chondrites are heavily altered, mainly consisting of fine-grained feldspathoids and FeO-rich spinel without melilite. The absence of melilite should be due to secondary reaction, because this mineral is one of the most abundant constituents of Ca-Al-rich inclusions and partial replacement of melilite by fine-grained feldspathoids is common in carbonaceous chondrites (e.g., MacPherson and Grossman 1984). This is supported by the higher Na and K contents and lower Ca content of the bulk RIs in comparison with those in carbonaceous chondrites (e.g., Ningqiang and Yamato-81020 in Fig. 2), and is consistent with previous reports (Kimura et al. 2002). Spinel is the most common component in the RIs, but typical of high FeO-enrichment. The composition of spinel varies continuously to magnesiochromite (Fig. 3). Furthermore, the spinel is ZnO-bearing, similar to FeO-rich spinel grains in other meteorites (Kimura et al. 2002; Lin and Kimura 2003; Dai et al. 2004). Ilmenite, instead of perovskite, occurs as small grains in spinel and the fine-grained alteration assemblages, suggesting formation of replacing perovskite. The high FeO and ZnO contents of spinel and the occurrence of ilmenite suggest oxidizing conditions for the alteration reactions. Similarly, RIs in enstatite chondrites are intensely altered. However, the alteration reactions are characteristic of highly reducing conditions as indicated by presences of Ti-rich sulfides and FeO-free spinel and lack of hedenbergite and andradite (Fagan et al. 2000; Guan et al. 2000c; Lin et al. 2003). This is consistent with the extremely reducing features of the host meteorites.

Phyllosilicates are commonly found in the alteration assemblages of RIs in Murchison and GRV 020025 CM2 chondrites, suggesting aqueous reactions in the nebula and/or the parent body. Except for the compact type A inclusions, other RIs in Allende found in this study are intensely altered too, consistent with previous reports of fluffy type A

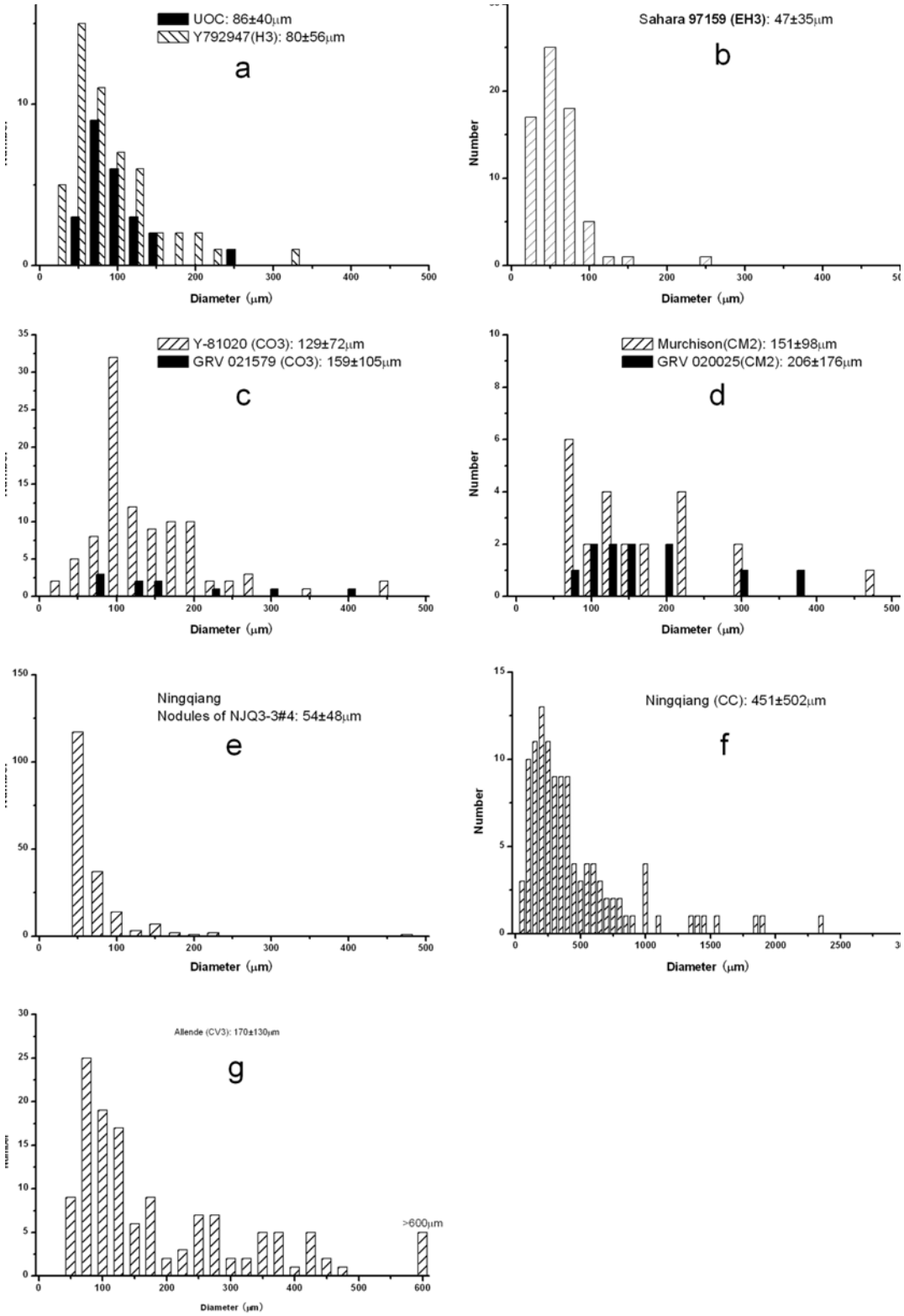

Fig. 5. Size distribution patterns of RIs in (a) ordinary chondrites studied in this work (UOC) and Y-792947 (H3) (Kimura et al. 2002), (b) Sahara 97159 (EH3) (Lin et al. 2003), (c) Y-81020 (CO3) and GRV 021579 (CO3) (Dai et al. 2004), (d) Murchison (CM2) and GRV 020025 (CM2) (Dai et al. 2004), (f) Ningqiang (CV3-like) (Lin and Kimura 2003) and (g) Allende (CV3). The two millimeter-sized RIs in Allende are excluded from the average value of the RIs. (e) The size distribution of individual concentric nodules in a Ningqiang refractory inclusion (NQJ3-3#4) is also shown for comparison. Three type Bs, two POIs and one type C inclusions in Ningqiang are not included. Note closely similar size distribution patterns of RIs in various chondrites and the nodules in the Ningqiang inclusion. The larger sizes of RIs in Allende and Ningqiang can partly be related to their common assemblages of numerous nodules.

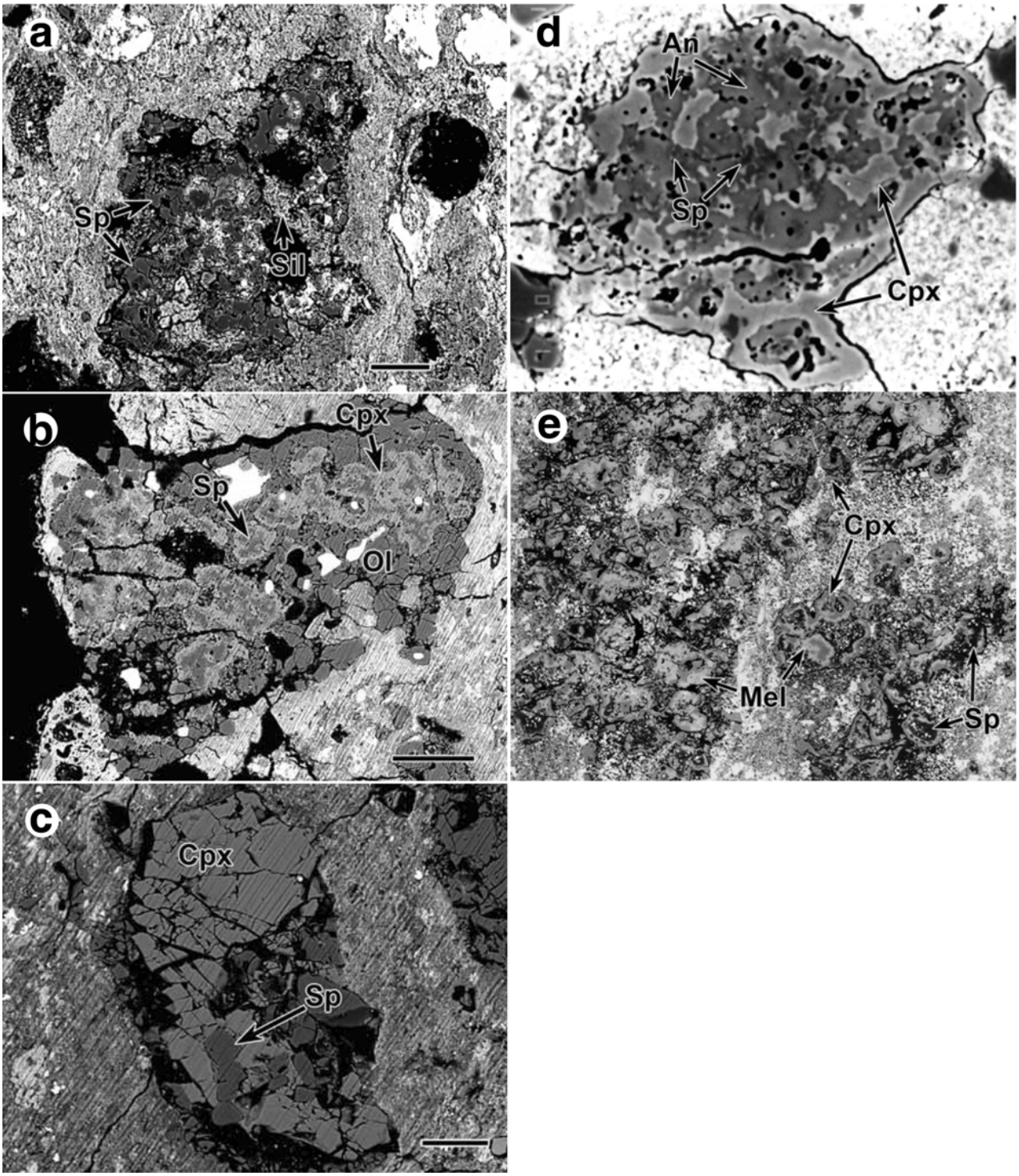

Fig. 6. BSE images of RIs in carbonaceous chondrites: a) Type A-like inclusion in Murchison (CM2) consisting of irregular grains of spinel (Sp) and fine-grained alteration assemblages (common phyllosilicates, Sil); width of 350 μm. b) Spinel-pyroxene inclusion in Murchison consisting of several concentric nodules surrounded by olivine (Ol) layers. Each nodule has a spinel core and a Ca-pyroxene rim (Cpx). Width 640 μm. c) Spinel-pyroxene fragment in Murchison with several euhedral grains of spinel enclosed in coarse-grained Ca pyroxene (Cpx), different from the spinel-pyroxene inclusion shown above; width 80 μm. d) Anorthite-pyroxene-rich inclusion in Yamato-81020 (CO3) consisting mainly of anorthite (An) and Ca-rich pyroxene (Cpx) with minor amount of spinel (Sp); width 80 μm; e) Micrograph of a part of a fluffy type A inclusion (NQJ3-3#4) in the Ningqiang carbonaceous chondrite (Lin and Kimura 2003), which is a loosely packed assemblage of numerous concentric nodules. The nodules consist of melilite (Mel) and spine cores and Ca-pyroxene rims. Note weak alteration of melilite; width 680 μm.

inclusions in the same meteorite (MacPherson and Grossman 1984). In contrast, RIs in Yamato-81020 CO3 chondrite do not show significant alteration, but commonly contain anorthite. This was confirmed by Itoh et al. (2004). The anorthite could be produced by reaction of melilite with nebular gaseous components earlier than formation of type C inclusions. The similar assemblages were found in Ningqiang and they are proposed to be precursors of type C inclusions (Lin and Kimura 1998). Similar to the RIs in Ningqiang and Yamato-81020, those in the unique carbonaceous chondrite Acfer 094 (Krot et al. 2004b) and in some CR chondrites contain little secondary feldspathoids, but commonly have abundant anorthite replacing melilite (Aléon et al. 2002; Krot et al. 2002).

Initial Mineral Assemblages of Highly Altered Refractory Inclusions

In order to compare petrographic type distributions of RIs in various chondrites, it is important to determine initial mineral assemblages of the highly altered RIs. These RIs mainly consist of fine-grained alteration products and spinel ± Ca pyroxene, with little melilite remaining. As discussed above, the fine-grained assemblages are likely alteration products of melilite that is one of the major constituent phases of Ca-Al-rich inclusions. Hence, the precursor of the fine-grained assemblages can usually be referred to as melilite. In contrast, spinel and less abundant hibonite are resistant to the secondary alteration, as indicated by their occurrences in the highly altered RIs in various chondrites. Altered perovskite can be recognized by occurrence of ilmenite in carbonaceous and ordinary chondrites or Ti-rich phases in enstatite chondrites. Ca pyroxene might be partially altered, but relict grains are commonly found (e.g., the remaining Wark-Lovering rims). Anorthite is ready to be altered like melilite, producing fine-grained feldspathoids (e.g., Lin and Kimura 1998). However, it is a secondary phase in type A and spinel-pyroxene inclusions. Primary anorthite usually occurs in the coarse-grained Ca-Al-rich inclusions of type B, C, and POI that contain coarse-grained Ca pyroxene. Accordingly, the mineral assemblages prior to alteration of RIs can be determined.

Furthermore, occurrences of spinel can tell more about the initial petrographic types of the highly altered RIs. The textural setting of spinel as small grains embedded in the fine-grained alteration assemblages is similar to that of spinel in fluffy type A inclusions, except that spinel is enclosed in melilite in the latter. Accordingly, these RIs are referred to as type A-like as described above. Spinel fragments are counted as spinel-pyroxene inclusions because they look similar to the spinel cores of the latter. Although relatively larger grain sizes and little fine-grained alteration products of the spinel fragments are inconsistent with a genetic link with type A inclusions, we cannot exclude a possibility that some of them may be fragments of Wark-Lovering rims of type As. However, this uncertainty is not significant, since there is a continuum between type A and spinel-pyroxene inclusions in modal and bulk compositions (Lin and Kimura 2003).

On the other hand, coarse-grained refractory inclusions, including compact type A, type B, C, and POI, contain euhedral grains of spinel, distinguished from the small and irregular to subhedral grains in fluffy type As and the irregular lumps in spinel-pyroxene inclusions. In addition, occurrence of relict Ca pyroxene is expected in alteration assemblages of type B, C, and POIs, which was not found in this study. Finally, the spinel fragments cannot either be from spinel-hibonite spherules that are well preserved in ordinary and enstatite chondrites and in Murchison.

Similar Petrographic Type Distributions

The survey of RIs in the 18 ordinary chondrites and in the Allende and Murchison carbonaceous chondrites, together with our previous data and literature, demonstrates that type A (or A-like) and spinel-pyroxene inclusions are the two dominant petrographic types in all chondrites summarized in Table 1. Although there are some uncertainties in the relative abundances of various petrographic types of RIs, type A (or A-like) and spinel-pyroxene inclusions are much more abundant than the other types and such a difference cannot be contributed to the errors.

The most intensely and extensively studied RIs in CV chondrites, especially in Allende, are coarse-grained inclusions, such as types B, C and POI, and compact type A. This gave an impression of high abundances of the coarse-grained inclusions in these meteorites. However, our unbiased survey of 4 sections of Allende reveals that almost all of the RIs are type A and spinel-pyroxene inclusions, except for a hibonite-rich inclusion and another hibonite-spinel fragment. Five CTAs have been identified in the sections, but there were no types B, C, or POI. The absence of these coarse-grained inclusions could be due to heterogeneous sampling. Occurrence of the coarse-grained inclusions in CV chondrites and rareness in other carbonaceous chondrites could be related to size sorting, because the coarse-grained RIs are compatible in size with chondrules in CVs, but much larger than those in other carbonaceous chondrites.

Analogically, hibonite-rich inclusions are the most intensely studied RIs in CM chondrites (e.g., Ireland 1988), because hibonite is one of the earliest condensates and its typical blue color can be easily recognized. In addition, many spinel-hibonite spherules were separated from CM chondrites by freeze-saw method and density separation (e.g., MacPherson et al. 1983), hence they are not representative of RIs in these chondrites. The survey of two sections of Murchison conducted in this work reveals all of the RIs are type A-like and spinel-pyroxene except for one with euhedral grains of spinel enclosed in coarse-grained Ca pyroxene. This

is consistent with our previous study of RIs in GRV 020025 (CM2) (Dai et al. 2004). MacPherson and Davis (1994) reported 66 spinel-rich inclusions in Mighei (CM2). Most of them are spinel-pyroxene, and many of the others are similar to type A-like if the fine-grained assemblages are alteration products of melilite.

It is also noticed that relative abundance ratios between type A (or A-like inclusions) and spinel-pyroxene inclusions may vary among chondrites (Table 1). The variation may partly be due to assignment of the petrographic types because they are continuous in both petrography and bulk compositions (Lin and Kimura 2003). CH chondrites contain more hibonite and/or grossite-rich inclusions. Krot et al. (2006) reported 23 hibonite/grossite-rich inclusions out of 50 refractory inclusions in NWA 739 (CH). The unique carbonaceous chondrite Acfer 094 also has a high abundance of hibonite/grossite-rich inclusions in 19 out of 132 inclusions (Krot et al. 2004b). The hibonite/grossite-bearing, type A, and spinel-pyroxene inclusions represent continuous condensate assemblages of the solar nebula from high to low temperature because of their bulk compositions in Ningqiang following condensation trajectory of the solar nebula (Lin and Kimura 2003). The hibonite/grossite-rich inclusions could be the first condensate assemblages because both hibonite and grossite are the earliest condensates of the solar nebular (Fegley 1991; Yoneda and Grossman 1995). The variation of relative abundance ratios of hibonite/grossite-rich, type A, and spinel-pyroxene inclusions probably indicates their continuous transportation during the condensation process in the solar nebula. It is unlikely that RIs can be selectively sampled by certain chondrites based on different mineral assemblages, unless they show systematic differences in sizes, density, or formation time and location.

Another difference is common occurrence of the fine-grained anorthite-spinel-rich inclusions in the Ningqiang carbonaceous chondrite and their counterparts in some CO and CR chondrites (Table 1). However, as discussed above, the anorthite is not a primary phase but was produced by reaction of melilite in the precursor type A inclusions with the nebular gas. It is unclear whether the reaction took place during the condensation processes or after these inclusions had been moved to the host chondrite accreting locations. The first possibility is consistent with variation in the relative abundance ratios between hibonite/grossite-rich, type A and spinel-pyroxene inclusions from different chondrites as discussed above. However, no ^{26}Mg excess was found in anorthite in an ASI from Ningqiang (Lin et al. 2005), which suggests a minimum time interval of 1.5 Ma after the first formation of RIs. Furthermore, the anorthite and feldspathoids in the ASI show similar ^{16}O-poor isotopic compositions, different from the unaltered melilite-spinel crust of the same inclusion (Guan et al. 2005), which suggests that both anorthite and feldspathoids formed in a same oxygen reservoir distinct from formation location of the primary minerals. These isotopic observations suggest late formation of anorthite after transportation from their resource. Alternatively, the absence or rareness of fine-grained anorthite-spinel-rich inclusions in other chondrites may be related to their high degree of secondary alteration, with feldspathoids and/or phyllosilicates replacing anorthite and/or melilite. This is consistent with the observation that chondrites with higher abundance of ASIs are usually little altered.

Compatible Size Distributions

The size distribution patterns of RIs in various chondrites are closely similar to each other. All of the 24 RIs in the ordinary chondrites are small in size. They have a nearly identical size distribution pattern with that of a total of 66 RIs in the three paired H3 chondrites (Fig. 5a), which suggests that the size distribution patterns of RIs in ordinary chondrites are not related with their abundances. Hence, these data can be summarized together and give an average size of 82 ± 52 μm. This result is consistent with previous reports of a few small RIs in other ordinary chondrites (Bischoff and Keil 1983; Kornacki and Fegley 1984; Guan et al. 2000b; Huss et al. 2001). For comparison, size distribution of 66 RIs in the Sahara 97159 EH3 chondrite has a similar pattern too (Fig. 5b). This is confirmed by studies of RIs in other enstatite chondrites. Guan et al. (2000c) reported a total of 80 RIs in 6 enstatite chondrites, with the majority <50 μm and the maximum of 120 μm in diameter, and Fagan et al. (2000) found 13 RIs with diameters of 30–80 μm in enstatite chondrites. The new data reveal that RIs in ordinary and enstatite chondrites are small in size and share similar size distribution patterns.

It is generally considered that RIs, similar to chondrules, show distinct size distributions among various groups of carbonaceous chondrites. Most of millimeter- and centimeter-sized RIs were found in CV3 chondrites and they are the most intensely studied objects in Allende. In contrast, RIs in CM2 and CO3 chondrites are usually sub-millimeters in size. However, such a difference was not based on a complete survey of RIs in these chondrites. Furthermore, many RIs in carbonaceous chondrites are loose assemblages of numerous individual concentric nodules. Conglomeration of the individual nodules has significant affection on size distribution of the RIs. This is demonstrated by the size distribution pattern of individual nodules of a millimeter-sized RI in Ningqiang, showing an average diameter of 54 ± 48 μm closely similar to that of RIs in ordinary and enstatite chondrites (Fig. 5e). Hence, we used sizes of the single inclusions and the individual nodules of other conglomerated inclusions instead of the whole assemblages in Allende and Murchison. The results are plotted in Fig. 5. We noticed that most RIs in the carbonaceous chondrites share the same size distribution pattern, closely similar to that of ordinary and

enstatite chondrites. Although RIs in the CV3 chondrites are somewhat larger in size, there is a peak at 75–125 μm. The relatively larger sizes of the RIs in CV3s may be explained by secondary growth through melting and annealing processes of loose assemblages of numerous nodules. The above observations are also supported by small sizes of RIs in other carbonaceous chondrites, e.g., 10–300 μm in MAC 87300 and 88107 (between CO3 and CM2) (Russell et al. 2000), ~50–400 μm in HH 237 and QUE 94411 (CH-like) (Krot et al. 2001), 25–185 μm (average 70 μm) in NWA 739 (CH) (Krot et al.), and <500 μm in CR chondrites (Aléon et al. 2002).

Similar Origins of Refractory Inclusions Among Chondrite Groups

As discussed above, regardless of various chemical groups of the host chondrites and their great heterogeneous abundances of RIs, our new data and available literature show basically similar distribution patterns of the petrographic types and sizes of RIs in various chondrites. The petrographic observation argues that RIs in various chemical groups of chondrites formed under similar processes and conditions, probably in the same region in the solar nebula. This is consistent with previous studies based on oxygen isotopes (McKeegan et al. 1998; Guan et al. 2000a; Fagan et al. 2001; Lin et al. 2003), Al-Mg isotopic system (Guan et al. 2000c; Huss et al. 2001), and rare earth elements (Lin et al. 2003), which suggest a same reservoir of RIs in ordinary and enstatite chondrites as those in carbonaceous chondrites. In contrast, if RIs had formed in locations where the host chondrites accreted, the primary mineral assemblages of the RIs should reflect different nebular conditions. Especially, highly reduced primary phases, such as oldhamite, niningerite, and carbides that condensed early under reduced conditions (Larimer and Bartholomay 1979), are expected in the RIs in enstatite chondrites. However, such mineral assemblages are never encountered in enstatite chondrite RIs.

During and/or after formation, RIs were transported to different locations where various groups of chondrites accreted. As discussed above, the alteration assemblages of RIs are related to the host meteorites, suggesting that the alteration reactions should have taken place in the host meteorite accreting locations, in the nebula and/or the asteroidal bodies. The intense alteration of RIs in all ordinary and enstatite chondrites may reflect large variation of physicochemical conditions between the RI reservoir and the chondrite-accreting locations. One possibility is that the ordinary and enstatite chondrites may have more distant spatial relationship with the RI reservoir in comparison with carbonaceous chondrites. Another hint for a remote relationship of ordinary and enstatite chondrites with the RI reservoir is the significantly lower abundances but high frequency of fragmentation of RIs in ordinary and enstatite chondrites than in carbonaceous chondrites.

CONCLUSIONS

A total of 24 RIs were found in ordinary chondrites. All of them are heavily altered with no melilite remaining, probably completely replaced by secondary minerals (nepheline and sodalite). This is confirmed by the higher Na_2O but lower CaO of the bulk RIs in comparison with those in little altered RIs in the Ningqiang and Yamato-81020 carbonaceous chondrites. The alteration should have taken place under oxidizing conditions, as indicated by FeO-ZnO-rich spinel and replacement of perovskite by ilmenite. However, most of the RIs found in this study and those in the three paired H3 chondrites (Yamato-792947, 793408 and 82038) had been characteristic of type A-like or spinel-pyroxene inclusions. They share similar size and petrographic type distribution patterns as those in enstatite chondrites.

A survey of RIs was conducted on Allende (CV3) and Murchison (CM2). This study and our previous data show that type A (or type A-like) and spinel-pyroxene inclusions are also the predominant types in various groups of carbonaceous chondrites, similar to the counterparts in ordinary and enstatite chondrites. Although some other carbonaceous chondrites, e.g., CH group, have higher relative abundance of hibonite and/or grossite-rich inclusions, this difference could be explained by continuous transport of RIs during condensation of the solar nebula, with the CH chondrites sampling more RIs that formed earlier. Many RIs in Allende and Murchison are loosely packed assemblages of numerous individual nodules, a major reason for their larger sizes in comparison with those in other carbonaceous chondrites and in ordinary and enstatite chondrites. The size distribution patterns of the single inclusions and the individual nodules of conglomerated ones in various carbonaceous chondrites are closely similar to each other and to those in ordinary and enstatite chondrites.

Compatible size and petrographic type distribution patterns of RIs in various chemical groups of chondrites argue for a same reservoir of RIs, consistent with previous studies of oxygen isotopes, Al-Mg isotopic systems and rare earth elements. During and/or after formation, RIs were transported into different locations and were altered there because of changing conditions.

Acknowledgments–We are grateful to A. N. Krot, T. J. Fagan, and H. Nagahara for their constructive reviews. The authors thank the Japanese National Institute of Polar Research and the Polar Research Institute of China for the sample allocation. This study was supported by the pilot project of knowledge innovation program of the Chinese Academy of Sciences (grant KZCX3-SW-123) and the National Natural Science Foundation of China (grant 40473038) (Y. Lin), and grant-in-aid for scientific Research from the Ministry of Education, Science and Culture of Japan, No. 16540435 (M. Kimura).

Editorial Handling—Dr. Hiroko Nagahara

REFERENCES

Aléon J., Krot A. N., and McKeegan K. D. 2002. Calcium-aluminum-rich inclusions and amoeboid olivine aggregates from the CR carbonaceous chondrites. *Meteoritics & Planetary Science* 37:1729–1755.

Bischoff A. and Keil K. 1983. Ca-Al-rich chondrules and inclusions in ordinary chondrites. *Nature* 303:588–592.

Bischoff A. and Keil K. 1984. Al-rich objects in ordinary chondrites: Related origin of carbonaceous and ordinary chondrites and their constituents. *Geochimica et Cosmochimica Acta* 48:693–709.

Dai D., Lin Y., Miao B., Shen W., and Wang D. 2004. Ca-, Al-rich inclusions in three new carbonaceous chondrites from the Grove Mountains, Antarctica: New evidence for a similar origin of the objects in various groups of chondrites. *Acta Geologica Sinica* 78:1042–1051.

Fagan T. J., Krot A. N., and Keil K. 2000. Calcium-aluminum-rich inclusions in enstatite chondrites I: Mineralogy and textures. *Meteoritics & Planetary Science* 35:771–781.

Fagan T. J., McKeegan K. D., Krot A. N., and Keil K. 2001. Calcium-aluminum-rich inclusions in enstatite chondrites II: Oxygen isotopes. *Meteoritics & Planetary Science* 36:223–230.

Fegley B., Jr. 1991. The stability of calcium aluminate minerals in the solar nebula (abstract). 22nd Lunar and Planetary Science Conference. pp. 367–368.

Grossman L. 1975. Petrography and mineral chemistry of Ca-rich inclusions in the Allende meteorite. *Geochimica et Cosmochimica Acta* 39:433–454.

Guan Y., McKeegan K. D., and MacPherson G. J. 2000a. Oxygen isotopes in calcium-aluminum-rich inclusions from enstatite chondrites: New evidence for a single CAI source in the solar nebula. *Earth and Planetary Science Letters* 181:271–277.

Guan Y., McKeegan K. D., and MacPherson G. J. 2000b. Oxygen-isotopic compositions in two calcium-aluminum-rich inclusions from unequilibrated ordinary chondrites (abstract). *Meteoritics & Planetary Science* 35:A67.

Guan Y., Huss G. R., MacPherson G. J., and Wasserburg G. J. 2000c. Calcium-aluminum-rich inclusions from enstatite chondrites: Indigenous or foreign? *Science* 289:1330–1333.

Guan Y., Huss G. R., MacPherson G. J., and Leshin L. A. 2002. Rare earth elements of calcium-aluminum-rich inclusions in unequilibrated enstatite chondrites: Characteristics and implications (abstract). *Meteoritics & Planetary Science* 37:A59.

Guan Y., Lin Y., and Leshin L. A. 2005. Oxygen isotope distribution in anorthite-spinel-rich inclusions from the Ningqiang carbonaceous chondrite (abstract #2027). 36th Lunar and Planetary Science Conference. CD-ROM.

Huss G. R., MacPherson G. J., Wasserburg G. J., Russell S. S., and Srinivasan G. 2001. ^{26}Al in CAIs and chondrules from unequilibrated ordinary chondrites. *Meteoritics & Planetary Science* 36:975–997.

Ireland T. R. 1988. Correlated morphological, chemical, and isotopic characteristics of hibonites from the Murchison carbonaceous chondrite. *Geochimica et Cosmochimica Acta* 52:2827–2839.

Ireland T. R. 1990. Presolar isotopic and chemical signatures in hibonite-bearing refractory inclusions from the Murchison carbonaceous chondrite. *Geochimica et Cosmochimica Acta* 54: 3219–3237.

Itoh S., Kojima H., and Yurimoto H. 2004. Petrography and oxygen isotopic compositions in refractory inclusions from CO chondrites. *Geochimica et Cosmochimica Acta* 68:183–194.

Kimura M., El Goresy A., Palme H., and Zinner E. 1993. Ca-, Al-rich inclusions in the unique chondrite ALH 85085: Petrology, chemistry, and isotopic compositions. *Geochimica et Cosmochimica Acta* 57:2329–2359.

Kimura M., Hiyagon H., Palme H., Spettel B., Wolf D., Clayton R. N., Mayeda T. K., Sato T., Suzuki A., and Kojima H. 2002. Yamato-792947, 793408 and 82038: The most primitive H chondrites, with abundant refractory inclusions. *Meteoritics & Planetary Science* 37:1417–1434.

Kojima T., Yada S., and Tomeoka K. 1995. Ca-Al-rich inclusions in three Antarctic CO3 chondrites, Yamato-81020, Yamato-82050 and Yamato-790992: Record of low-temperature alteration. *Proceedings of the NIPR Symposium on Antarctic Meteorites* 8: 79–96.

Kornacki A. S. and Fegley B., Jr. 1984. Origin of spinel-rich chondrules and inclusions in carbonaceous and ordinary chondrites. Proceedings, 15th Lunar and Planetary Science Conference. pp. B588–B596.

Krot A. N., McKeegan K. D., Russell S. S., Meibom A., Weisberg M. K., Zipfel J., Krot T. V., Fagan T. J., and Keil K. 2001. Refractory calcium-aluminum-rich inclusions and aluminum-diopside-rich chondrules in the metal-rich chondrites Hammadah al Hamra 237 and Queen Alexandra Range 94411. *Meteoritics & Planetary Science* 36:1189–1216.

Krot A. N., Meibom A., Weisberg M. K., and Keil K. 2002. The CR chondrite clan: Implications for early solar system processes. *Meteoritics & Planetary Science* 37:1451–1490.

Krot A. N., MacPherson G. J., Ulyanov A. A., and Petaev M. I. 2004a. Fine-grained, spinel-rich inclusions from the reduced CV chondrites Efremovka and Leoville: I. Mineralogy, petrology, and bulk chemistry. *Meteoritics & Planetary Science* 39:1517–1553.

Krot A. N., Fagan T. J., Keil K., McKeegan K. D., Sahijpal S., Hutcheon I. D., Petaev M. I., and Yurimoto H. 2004b. Ca, Al-rich inclusions, amoeboid olivine aggregates, and Al-rich chondrules from the unique carbonaceous chondrite Acfer 094: I. mineralogy and petrology. *Geochimica et Cosmochimica Acta* 68:2167–2184.

Krot A. N., Petaev M. I., Russell S. S., Itoh S., Fagan T. J., Yurimoto H., Chizmadia L., Weisberg M. K., Komatsu M., Ulyanov A. A., and Keil K. 2004c. Amoeboid olivine aggregates and related objects in carbonaceous chondrites: Records of nebular and asteroid processes. *Chemie der Erde* 64:185–239.

Krot A. N., Petaev M. I., and Keil K. 2006. Mineralogy and petrology of Al-rich objects and amoeboid olivine aggregates in the CH carbonaceous chondrite North West Africa 739. *Chemie der Erde* 66:57–76.

Larimer J. W. and Bartholomay M. 1979. The role of carbon and oxygen in cosmic gases: Some applications to the chemistry and mineralogy of enstatite chondrites. *Geochimica et Cosmochimica Acta* 43:1455–1466.

Lin Y. and Kimura M. 1998. Anorthite-spinel-rich inclusions in the Ningqiang carbonaceous chondrite: Genetic links with type A and C inclusions. *Meteoritics & Planetary Science* 33:435–446.

Lin Y. and Kimura M. 2003. Ca-Al-rich inclusions from the Ningqiang meteorite: Continuous assemblages of the nebular condensates and genetic link to type Bs. *Geochimica et Cosmochimica Acta* 67:2251–2267.

Lin Y., Kimura M., Hiyagon H., and Monoi A. 2003. Unusually abundant refractory inclusions from Sahara 97159 (EH3): A comparative study with other groups of chondrites. *Geochimica et Cosmochimica Acta* 67:4935–4948.

Lin Y., Kimura M., Miao B., and Dai D. 2004. Comparative study of refractory inclusions from different groups of chondrites (abstract). In Workshop on Chondrites and the Protoplanetary Disk. pp. 111–112.

Lin Y., Guan Y., Leshin L. A., Ouyang Z., and Wang D. 2005. Short-lived chlorine-36 in a Ca-Al-rich inclusion from the Ningqiang carbonaceous chondrite. *Proceedings of the National Academy of Sciences* 102:1306–1311.

Macdougall J. D. 1979. Refractory-element-rich inclusions in CM meteorites. *Earth and Planetary Science Letters* 42:1–6.

MacPherson G. J. and Grossman L. 1984. "Fluffy" type A Ca-, Al-rich inclusions in the Allende meteorite. *Geochimica et Cosmochimica Acta* 48:29–46.

MacPherson G. J. and Davis A. M. 1994. Refractory inclusions in the prototypical CM chondrite, Mighei. *Geochimica et Cosmochimica Acta* 58:5599–5625.

MacPherson G. J., Bar-Matthews M., Tanaka T., Olsen E., and Grossman L. 1983. Refractory inclusions in the Murchison meteorite. *Geochimica et Cosmochimica Acta* 47:823–839.

McKeegan K. D., Leshin L. A., Russell S. S., and MacPherson G. J. 1998. Oxygen isotopic abundances in calcium-aluminum-rich inclusions from ordinary chondrites: Implications for nebular heterogeneity. *Science* 280:414–418.

Russell S. S., Huss G. R., Fahey A. J., Greenwood R. C., Hutchison R., and Wasserburg G. J. 1998. An isotopic and petrologic study of calcium-aluminum-rich inclusions from CO3 meteorites. *Geochimica et Cosmochimica Acta* 62:689–714.

Russell S. S., Davis A. M., MacPherson G. J., Guan Y., and Huss G. R. 2000. Refractory inclusions from the ungrouped carbonaceous chondrites MAC 87300 and MAC 88107. *Meteoritics & Planetary Science* 35:1051–1066.

Sheng Y. J., Hutcheon I. D., and Wasserburg G. J. 1991. Origin of plagioclase-olivine inclusions in carbonaceous chondrites. *Geochimica et Cosmochimica Acta* 55:581–599.

Simon S. B., Davis A. M., Grossman L., and Zinner E. K. 1998. Origin of hibonite-pyroxene spherules found in carbonaceous chondrites. *Meteoritics & Planetary Science* 33:411–424.

Wark D. A. 1987. Plagioclase-rich inclusions in carbonaceous chondrite meteorites: Liquid condensates? *Geochimica et Cosmochimica Acta* 51:221–242.

Wark D. A. and Lovering J. F. 1982. The nature and origin of type B1 and B2 Ca-Al-rich inclusions in the Allende meteorite. *Geochimica et Cosmochimica Acta* 46:2581–2594.

Weber D. and Bischoff A. 1997. Refractory inclusions in the CR chondrite Acfer 059-El Djouf 001: Petrology, chemical composition, and relationship to inclusion populations in other types of carbonaceous chondrites. *Chemie der Erde* 57:1–24.

Yoneda S. and Grossman L. 1995. Condensation of CaO-MgO-Al_2O_3-SiO_2 liquids from cosmic gases. *Geochimica et Cosmochimica Acta* 59:3413–3444.